World Applied Sciences Journal 35 (8): 1530-1536, 2017
ISSN 1818-4952

DOI: 10.5829/idosi.wasj.2017.1530.1536

Shearing Interference Microscope for Step-Height Measurements

[1]*Hung-Xuβn Trinh,* [1]*Shyh-Tsong Lin,* [2]*Liang-Chia Chen,*
[3]*Sheng-Lih Yeh,* [4]*Chin-Sheng Chen and* [5]*Hong-Hai Hoang*

[1]Department of Electro-optical Engineering, National Taipei University of Technology,
[2]Department of Mechanical Engineering, National Taiwan University,
[3]Department of Mechanical Engineering, Lunghwa University of Science and Technology,
[4]Graduate Institute of Automation Technology, National Taipei University of Technology,
[5]School of Mechanical Engineering, Hanoi University of Science and Technology,
01 Dai Co Viet Street, Hanoi City, VietNam

Abstract: A shearing interference microscope using a Savart prism as the shear plate is proposed for inspecting step-heights. Where the light beam propagates through the Savart prism and microscopic system to illuminate the sample, it then turns back to re-pass through the Savart prism and microscopic system to generate a shearing interference pattern on the camera. Two measurement modes, phase-shifting and phase-scanning, can be utilized to determine the depths of the step-heights on the sample. The first mode, which employs a narrowband source, is based on the five-step phase-shifting algorithm and has a measurement range of a quarter-wavelength. The second mode, which adopts a broadband source, is based on peak-intensity identification technology and has a measurement range up to a few micrometers. This paper is to introduce the configuration and measurement theory of this microscope, perform a setup used to implement it and present the experimental results from the uses of the setup. The results not only verify the validity but also confirm the high measurement repeatability of the proposed microscope.

Key words: Shearing interferometer microscope・Phase-shifting・Phase-scanning・Step-height

INTRODUCTION

Surfaces patterned with step-heights ranging from several nanometers to serval micrometers have now widely exhibited in LCD displays, OLED displays, photovoltaic cells, integrated circuits and etc. To ensure the quality of these kinds of devices, precision instruments for examining the step-heights are now in great request. Three kinds of optical instruments have been approved to be qualified candidates, they are confocal microscopes (CMs), interference microscopes (IMs) and differential interference contrast microscopes (DICMs).

The CMs place two pin holes [1-4], one at the light source arm and the other at the sensor arm, at the conjugate points of the object. Their vertical resolution is hence significantly enhanced by comparing with the conventional microscopes, but their throughput is limited due to the required point-scanning measurement process. To circumvent the limitation, the line-scanning CMs have been developed successfully [5-9], their measurements are however still time consuming.

The IMs are based on the theory of optical interferometry and three major configurations, Michelson [10, 11], Mirau [12-15] and Linnik [16-19], of which have been verified to be useful in industrial applications. The IMs are with the advantages over the conventional microscopes of full-field detection and excellence in vertical resolution, they are however un-available in on-line examinations. The IMs are very sensitive to surrounding noise (vibration, sound and etc.), they are formally installed on tables capable of isolating the noise.

The DICMs [20-29] are based on the mutual interference of two identical wavefronts having a lateral distance smaller than the diameter of an Airy disk. Since they belong to the category of common-path configuration,

Corresponding Author: Hung-Xuân Trinh, Department of Electro-optical Engineering, National Taipei University of Technology.

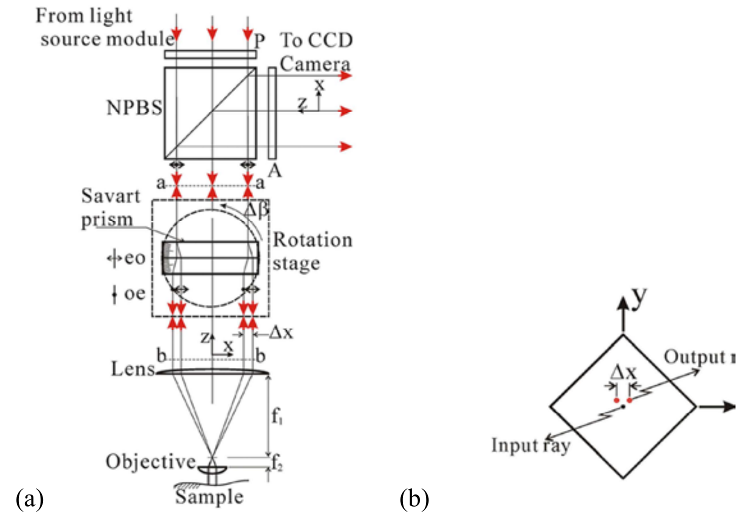

Fig. 1: (a) Schematic diagram of the proposed shearing interference microscope; (b) side view (along the positive z-axis) of the Savart prism in (a).

they are immune to surrounding perturbations. However, the detected phase is a function of the derivative of the object, they perform excellently only in edge detections.

An innovative shearing interference microscope (SIM) is therefore proposed for step-height measurements. Aside from performing the brilliant performance of IMs and DICMs (i.e., full-field detection, high vertical resolution and anti-perturbation), it possesses the advantage of having phase-shifting and phase-scanning measurement modes. In this paper, the configuration, measurement theory and experimental setup of the SIM are introduced sequentially. The experiments and experimental results accomplished by using of the setup are demonstrated and discussed thereafter. The paper finally concludes by summering the measurement concept and performance of the proposed microscope.

Configuration and Measurement Theory: A schematic diagram of the SIM is shown in Figure 1. It is composed of a polarizer (P, the transmission axis of which is inclined at 0° with respect to the x-axis), non-polarized beam-splitter (NPBS), Savart prism, lens with a focal length of f_1, objective with a focal length of f_2, analyzer (A, the transmission axis of which is inclined at 0° relative to the x-axis), CCD camera and rotation stage. Where the Savart prism is placed on the rotation stage and pivoted so that its surface normal is oriented at a small angle, $\Delta\beta$, with respect to the positive z-axis. The lens and objective form an afocal microscopic system (AMS) having a lateral magnification of $\mathbf{M=-f_1/f_2}$.

Figure 1 also reveals that a collimated light beam from a light source module (LSM) is laterally sheared into two parallel beams, i.e. eo- and oe-beams, by the Savart prism. The sheared beams then travel to the sample under test and return to the Savart prism where they are counter-sheared. And the counter-sheared beams finally propagate through the analyzer to generate an interference pattern on the CCD camera.

For interpreting the meaning of the interference pattern, the wavefront evolution in the microscope is demonstrated in advance. As those shown in Figure 2, where (a) represents the wavefront of the beam moving down to the a-a plane (Figure 1); (b) shows the wavefronts of the sheared beams moving down to the b-b plane (Figure 1), the $\mathbf{\Lambda_s}$ and $\mathbf{\Delta}$x of which are optical path difference (OPD) and shear distance, respectively, due to the transmission of the beams through the Savart prism; (c) displays the wavefronts of the beams moving up to the b-b plane, the superimposed function of $\boldsymbol{W(x,y)}$ comes from the round trip of the beams to the sample; and (d) depicts the wavefronts of the beams moving up to the a-a plane, the counter-shear and OPD increment are caused by the reverse transmission of the beams through the Savart prism. Whereupon, the OPD of the beams propagating to the CCD camera is

$$\begin{aligned}\Lambda &= 2[\mathbf{W}(\mathbf{x}+\Delta\mathbf{x}/2,\mathbf{y})-\mathbf{W}(\mathbf{x}-\Delta\mathbf{x}/2,\mathbf{y})+\Lambda_{\mathbf{S}}] \\ &= 2(\Delta\mathbf{W}(\mathbf{x},\mathbf{y})+\Lambda_{\mathbf{S}})\end{aligned} \tag{1}$$

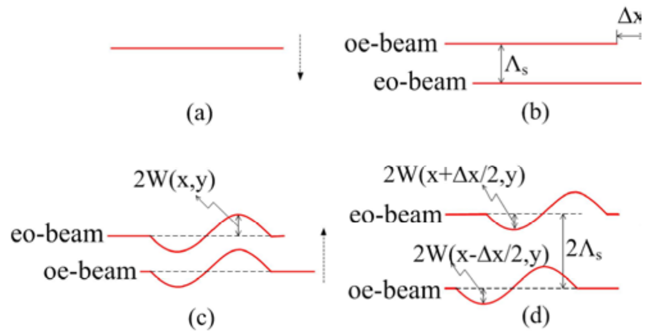

Fig. 2: Wavefront evolution in the shearing interference microscope.

where ***W(x,y)*** represents the contour of the sample, **Δ*W(x,y)*** denotes contour variation and $\mathbf{\Lambda_s}$ has an approximation, i.e. the higher order terms of **Δβ** are eliminated, of [30, 31]

$$\Lambda_s = \Delta x \cdot \Delta\beta \tag{2}$$

The preceding demonstration indicates that the OPD of the interference beams is contributed merely by the rotation of the Savart prism and the contour of the sample; this is small and permits a low-coherence source to produce observable interference. Furthermore, the interference pattern can be expressed as [32, 33]

$$I = I_0[1 + \gamma\cos(\phi_w + \delta)] \tag{3}$$

where $\mathbf{I_o}$ is background intensity, $\boldsymbol{\gamma}$ denotes fringe contrast and $\boldsymbol{\phi_w}$ + **Δ** is the phase corresponding to **Λ**. Let the central wavelength of the source be symbolized as $\mathbf{\Lambda_c}$, $\boldsymbol{\phi_w}$ and **Δ** have forms of

$$\phi_w = \frac{4\pi}{\lambda_c}\Delta W(x,y) \tag{4}$$

and

$$\delta = \frac{4\pi}{\lambda_c}\Lambda_s \cong \frac{4\pi}{\lambda_c}\Delta x \times \Delta\beta \tag{5}$$

Evidently, the pattern is the so-called shearing interference pattern and it involves the information of **Δ*W(x,y)***. To extract **Δ*W(x,y)*** from the pattern, two measurement modes are proposed.

Phase-shifting Measurement Mode: When the bandwidth of the source is narrow, $\boldsymbol{\gamma}$ can be regarded as a constant and this enables the microscope to extract the contour variation using the phase-shifting technology [32, 34]. It shifts the phase of the interference pattern by **δ** by rotating the Savart prism by **Δβ**, gets $\boldsymbol{\phi_w}$ by the use of

$$\phi_w = \tan^{-1}\left[\frac{2(I_2 - I_4)}{2I_3 - (I_1 + I_5)}\right] \tag{6}$$

and converts $\boldsymbol{\phi_w}$ into **Δ*W(x,y)*** using Eq. (4). Where $\mathbf{I_1}$, $\mathbf{I_2}$, $\mathbf{I_3}$, $\mathbf{I_4}$ and $\mathbf{I_5}$ are the interference patterns corresponding to phase shifts of -ππ, -ππ/2, 0, ππ/2 and ππ, respectively.

In fact, the atan2 function [35], which is with principal value in the range (-π,_π], is adopted to replace the arctan function in Eq. (6). The obtained $\boldsymbol{\phi_w}$, however, still contains 2π_discontinuities and is referred to as the wrapped phase map. Therefore, during the procedure of retrieving **Δ*W(x,y)***, a phase unwrapping technique [36] is also used for removing the discontinuities.

The phase-shifting mode fails if the sample has step-heights larger than a quarter-wavelength [34, 36]. To overcome this limitation, the phase-scanning mode introduced as follows can be employed.

Phase-scanning Measurement Mode: When the bandwidth of the source is wide (e.g., the bandwidth of a white light source), $\boldsymbol{\gamma}$ becomes an envelope function and peaks sharply at **Λ** = 0. This, as well as Eq. (3), indicates that the peak-intensity of every image point emerges while **Λ** = 0; accordingly, the contour variation can be obtained according to

$$\Delta W(x,y) = -\Delta x \cdot \Delta\beta_c \tag{7}$$

Here, $\mathbf{\Delta\beta_c}$ denotes the rotation angle of the Savart prism corresponding to the emergence of peak-intensity. The phase-scanning mode is to examine contour variation using the aforementioned characteristic. It instructs the rotation stage to carry the Savart prism to experience an angular scanning, records $\mathbf{\Delta\beta_c}$'s of all image points and substitutes the recorded $\mathbf{\Delta\beta_c}$'s into Eq. (7) to yield **Δ*W(x,y)***.

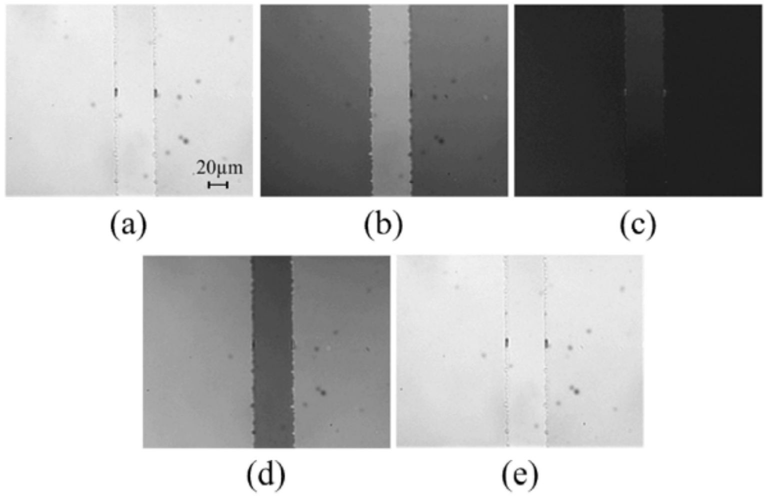

Fig. 3: (a), (b), (c), (d) and (e): The interference patterns corresponding to phase-shifts of -ππ, -ππ/2, 0, ππ/2 and ππ, respectively.

Experimental Setup: To implement the measurement concepts introduced in this paper, a setup composed of an LSM, the proposed SIM and a control and image processing system was installed. The LSM, which consists of a halogen lamp, a color filter and three lenses, radiates a nearly collimated light beam, which has a central wavelength Λ_c of 633 nm and full width at half maximum of 10 nm, to the SIM. As the filter is withdrawn, the output becomes a broadband source.

The SIM is configured as that shown in Figure 1. Of which, the Savart prism is made of calcite crystal and has a separation capability of Δx = 0.75 mm. The AMS has a lateral magnification of -20 (the lens and objective have focal lengths of 200 mm and 10 mm, respectively and the objective is 20X Nikon CFI 60 TU Plan Epi ELWD infinity corrected objective). And the rotation stage (NS5311-C, Nano Control Co., Ltd., Japan), which is equipped with a PZT actuator and capacitive sensor, has a rotation range of 800 arc-sec and a positioning resolution of 0.01 arc-sec.

The control and image processing system comprises a frame grabber, stage controller and driver and personal computer. Among them, the personal computer uses the frame grabber to capture interference images on the camera, communicates with the rotation stage via the stage controller and driver and executes measurement and display programs. The measurement program acquires contour variation using the phase-shifting or phase-scanning measurement mode and the display program displays the measurement results on the screen of the computer.

Experimental Results: If the sample has step-heights and the shear of the microscope brings the wavefront segments of the step-heights to interfere with the wavefront portion of the base plane, the measured $\boldsymbol{\Delta W(x,y)}$ contains the depths of the step-heights. This fact prompted the authors to validate the proposed microscope by conducting the experimental setup to examine two step-height samples. The first one, which was made from two reflective thin film layers on Silicon substrate (bottom layer was coated at full area and top layer was coated at half area) with different thickness, having a nominal step-height of 32nm; the second one, which was fabricated by Instrument Technology Research Center (ITRC), National Applied Research Laboratories, Taiwan, is a 2D rectangular grating having a period of 100_μm and a nominal step-height of 550nm.

Since the first sample has a nominal depth smaller than a quarter-wavelength, the phase-shifting measurement mode was employed during its examination. The results are shown in Figures 3 and 4.

Where Figures 3(a), (b), (c), (d) and (e) depict the five interference patterns corresponding to phase shifts of -ππ, -ππ/2, 0, ππ/2 and ππ, respectively; Figure 4(a) shows the contour variation obtained from the use of these five patterns; and Figure 4(b) presents the cross-section at y = 100 μm of Figure 4(a). From Figure 4(b), it is found that the examination exports a depth of 33.5 nm, which is consistent with that (32.5 nm) measured using an atomic force microscopy (AFM) with an area of 100x100 μm. The preceding examination was actually repeated for

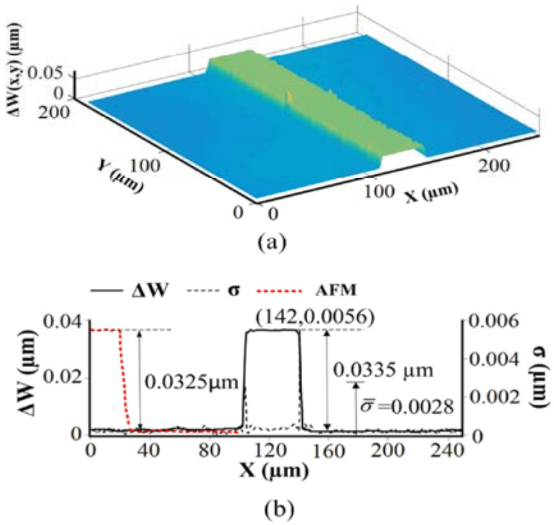

Fig. 4: (a) The measured $\Delta W(x,y)$ of the first sample; (b) the cross-section at y = 100μm of (a).

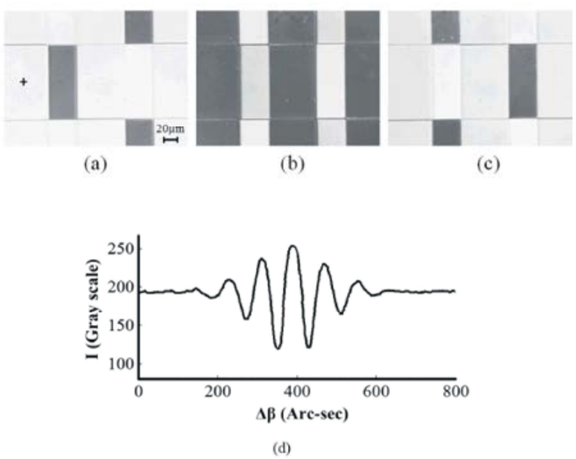

Fig. 5: (a), (b) and (c): The interference patterns corresponding to scanning angles of 200, 350 and 500 arc-sec, respectively; (d) the correlogram at the point + shown in (a).

30 times and the results were then conducted to calculate the standard deviation (σ) of the examination. Figure 4(b) also shows the calculated standard deviation with respect to the points of the same line and it indicates that the standard deviation has a maximum of 5.6 nm and an average ($\bar{\sigma}_c$) of 2.8 nm. Applying a medium filter to the measured data can eliminate the noise and accordingly reduce the standard deviation.

The nominal depths of the step-heights of the second sample are larger than a quarter-wavelength; hence, the phase-scanning mode was used to examine this sample. The results are presented in Figures 5 and 6.

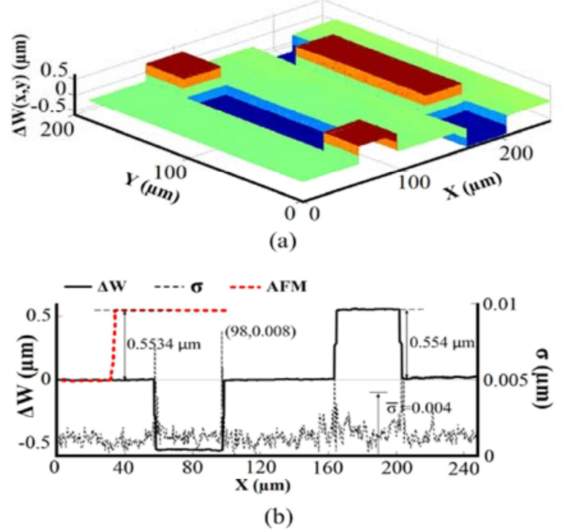

Fig. 6: (a) The measured $\Delta W(x,y)$ of the 2D rectangular grating; (b) the cross-section at y = 100 μm of (a). The rectangular coordinates, (x,y), in (a) have been moved onto the least-squares plane of the measured data.

Where Figures 5(a), (b) and (c) display the interference patterns captured at the scanning angles of 200, 350 and 500 arc-sec, respectively; Figure 5(d) exhibits the correlogram (i.e., plot of intensity versus scanning angle) of the point + marked in Figure 5(a), it demonstrates that every effective point has a distinguishable maximum value in intensity. Accordingly, the contour variation of every point can be retrieved without ambiguity by using the phase-scanning measurement mode.

Figure 6(a) displays the measured $\Delta W(x,y)$ and Figure 6(b) presents the cross-section at y = 100 μm of Figure 6(a). Figure 6(b) demonstrates that the examination outputs a height of 554nm, this is agreed by that (553.4nm) measured using AFM with an area of 100x100 μm.

Similar as those done for the first sample, the standard deviation of this examination was determined as well, of which the part with respect to the points of y = 100 μm of Figure 6(a) is drawn out and presented in Figure 6(b). In addition, the maximum and average of the presented standard deviation are revealed, it is found that they are 8 and 4 nm, respectively. The use of a medium filter can also shrink the standard deviation, but an increment of stepping angle of the angular scanning may enlarge it.

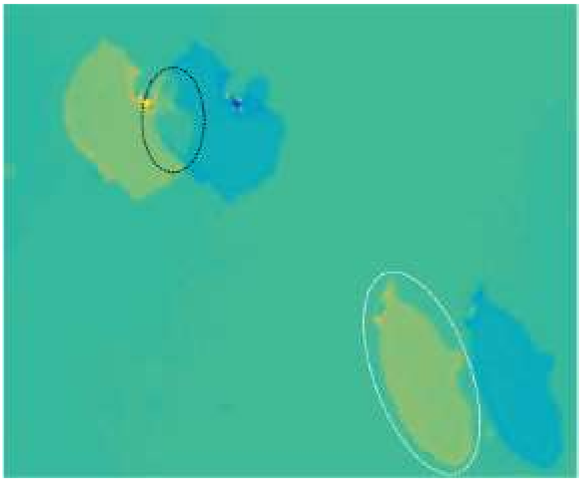

Fig. 7: The top view of measured contour variations of two samples, where the large and small samples are marked by black and white dashed line, respectively.

DISCUSSIONS

Apart from the preceding analysis, some recommendations on the uses of the microscope are provided as follows. The measurement range of the constructed SIM is 1.5 µm, this is small but not the limit of the proposed microscope. Replacing the rotation stage by that having a large rotation range and with a high sensitivity sensor, e.g. a rotation stage driven by a compound driver (stepper motor and PZT actuator) and equipped with a laser encoder would provide the microscope the ability of inspecting larger contour variation.

And, in the validity verification, the microscope was utilized to examine contour variations in the direction of x-axis; this may be insufficient since inspections for the orthogonal direction (i.e. y-axis) may be demanded as well in real applications. Once the rotation stage and Savart prism are rotated, from the situation shown in Fig.1, about the z-axis by 90 deg., the microscope is capable of inspecting contour variations in the direction of y-axis.

Moreover, the experimental results are only shown the height value of the step-height samples because of the shear distance is smaller than the size of sample. When the shear distance is bigger than the size of samples, the profile of the step-height samples can be obtained as shown in Figure 7. The top side of Figure 7 shows two contour variations of the sample which are overlap (indicated by black dashed line); therefore, there is unable to get the full profile of the sample. But in the bottom side of Figure 7, two contour variations of the other sample are totally separated; therefore, the full profile of the sample that is indicated by white dashed line can be directly extracted.

Furthermore, the measurement time of the proposed SIM is much shorter than CM. For one measurement with the same size of sample (250x180µm), the line-scanning CM is needed 16400 seconds, while the phase-shifting and phase-scanning measurement modes are needed 2 and 60 seconds, respectively.

CONCLUSIONS

In summary, this paper has introduced a novel low coherence light source shearing interference microscope for examining the step-height measurements using two measurement modes: phase-shifting and phase-scanning, presented a setup installed for realizing the microscope and demonstrated the experiments of employing the setup to examine two samples. The first sample is with a step-height having a nominal depth of 32nm, the examination with respect to this sample exports a measurement depth of 33.5nm and an average standard deviation of 2.8nm; and the second sample is a 2D rectangular grating having a nominal depth of 550nm, the examination corresponding to this grating outputs a measurement depth of 554nm and an average standard deviation of 4nm. The experimental results not only agree the validity but also confirm the high measurement repeatability of the proposed microscope.

REFERENCES

1. Hamilton, K. and T. Wilson, 1982. Surface profile measurement using the confocal microscope. J. Appl. Phys., 53: 5320-5322.
2. Minsky, M., 1988. Memoir on inventing the confocal microscope. Scanning, 10: 128-138.
3. Wilson, T. and A.R. Carlini, 1988. Three dimensional imaging in confocal imaging systems with finite-sized detectors. J. Microsc, 141: 51-66.
4. Sheppard, C.J.R. and D.M. Shotton, 1997. Confocal laser scanning microscopy. Springer-Verlag New York.
5. Dwyer, P.J., C.A. DiMarzio, J.M. Zavislan, W.J. Fox and M. Rajadhyaksha, 2006. Confocal reflectance theta line scanning microscope for imaging human skin in vivo. Opt. Lett., 31: 942–944.
6. Dwyer, P.J., C.A. DiMarzio and M. Rajadhyaksha, 2007. Confocal theta line-scanning microscope for imaging human tissues. Appl. Opt., 46: 1843-1851.

7. Simon, B. and C.A. Dimarzio, 2007. Simulation of a theta line-scanning confocal microscope. J. Biomed. Opt, 12: 064020.
8. Gareau, D.S., S. Abeytunge and M. Rajadhyaksha, 2009. Line-scanning reflectance confocal microscopy of human skin: comparison of full-pupil and divided-pupil configurations. Opt. Lett., 34: 3235-3237.
9. Patel, Y.G., M. Rajadhyaksha and C.A. DiMarzio, 2011. Optimization of pupil design for point-scanning and line-scanning confocal microscopy. Biomed. Opt. Exp., 8: 2231-2242.
10. Hernández. K., R. Rodríguez-Vera and J. Rayas, 2011. Michelson microscope interference objective for micro-structure topography measuring. Proc. of SPIE, 8011: 80117U.
11. Kühnhold. P, W. Xie and P. Lehmann, 2013. Comparison of Michelson and Linnik interference microscopes with respect to measurement capabilities and adjustment efforts. Proc. of SPIE, 8788: 87882G.
12. http://www.optics.arizona.edu/jcwyant.
13. Kino, G.S. and S.S.C. Chim, 2010. Mirau correlation microscope. Appl. Opt., 29: 3775-3783.
14. Bian, Y. and T. Guo, 2010. Step height evaluation in the vibrating condition based on microscopic interferometry. Proc. of SPIE, 7656: 76562H.
15. Smith, D., S. Singh, Y. Ramnath, M. Rabie, D. Zhang and L. England, 2004. TSV residual Cu step height analysis by white light interferometry for 3D integration. IEEE Electronic Components & Technology Conference, pp: 578-584.
16. Gale, D.M., M.I. Pether and J.C. Dainty, 1996. Linnik microscope imaging of integrated circuit structures. Appl. Opt., 35: 131-148.
17. Dubois, A., L. Vabre, A.C. Boccara and E. Beaurepaire, 2002. High-resolution full-field optical coherence tomography with a Linnik microscope. Appl. Opt., 41: 805-812.
18. Shuzhen, W., X. Tiebanga and C. Suping, 2010. Vertical scanning white light interfering profilometer based on Linnik interference microscope. Proc. of SPIE, 7656: 76563I.
19. Guo, H., L. Liu, X. Hao, K. Niu and X. Chou, 2011. Profile measurement system based on linnik-type interferometric microscope for visible-light region and infrared-light region. O pt. Laser Technol., 43: 1184-1189.
20. Sommargren, G.E. and B.J. Thompson, 1973. Linear phase microscopy. App. Opt., 12: 2130-2138.
21. Lessor, D.L., J.S. Hartman and R.L. Gordon, 1979. Quantitative surface topography determination by Nomarski reflection microscopy. 1. Theory. J. Opt. Soc. Am., 69: 357-366.
22. Hartman, J.S., R.L. Gordon and D.L. Lessor, 1980. Quantitative surface topography determination by Nomarski reflection microscopy. 2: Microscope modification, calibration and planar sample experiments. App. Opt., 19: 2998-3009.
23. Hartman, J.S., R.L. Gordon and D.L. Lessor, 1981. Nomarski differential interference contrast microscopy for surface slope measurements: an examination of techniques. App. Opt., 20: 2665-2669.
24. Wickramasinghe, H.K., S. Ameri and C.W. See, 1982. Differential phase contrast optical microscope with 1 A-depth resolution. Electron. Lett., 18: 973-975.
25. Jabr, S.N., 1985. Surface-roughness measurement by digital processing of Nomarski phase-contrast images. Opt. Lett., 10: 526-528.
26. Salmon, T., R.A. Walker and N.K. Pryer, 1989. Video-enhanced differential interference contrast light microscopy. Bio. Tech., 7: 624-633.
27. Ooki, H., Y. Iwasaki and J. Iwasaki, 1996. Differential interference contrast microscope with differential detection for optimizing image contrast. App. Opt., 35: 2230-2234.
28. Gleyzes, P., A.C. Boccara and H. Saint-Jalmes, 1997. Multichannel Nomarski microscope with polarization modulation: Performance and applications. Opt. Lett., 22: 1529-1531.
29. Munro, P.R.T. and P. Török, 2005. Vectorial, high numerical aperture study of Nomarski's differential interference contrast microscope. Opt. Express, 13: 6833-6847.
30. Francon, M and S. Mallick, 1971. Polaized Interferometer. John, W and Sons, Inc.
31. Guo, X., A. Zeng and H. Huang, 2008. Spatial phase-shifting lateral shearing interferometer. Proc. of SPIE, 7160: 71602D.
32. Gasvik, K.J., 2002. Interference. In Optical Metrology, Ed., John, W and Sons, pp: 37-65.
33. Hecht, E., 2002. In Optics, Ed., Addison. W, pp: 385-442.
34. Creath, K., 1998. Phase shifting to improve interferometry. In Optical method of engineering analysis edited by G. L. Cloud, Cambridge University Press, Cambridge, UK, pp: 477-491.
35. http://en.wikipedia.org/wiki/Atan2.
36. Macy, W.W., 1983. Two-dimensional fringe-pattern analysis. Appl. Opt., 22: 3898-3901.